Key Points:
- Forcing-induced uncertainty in the estimation of ET and runoff is considerable
- ET is dominated by T in the north and P in the south during growing season

Correspondence to:
Q. Zhuang,
qzhuang@purdue.edu

Evapotranspiration in Northern Eurasia: Impact of forcing uncertainties on terrestrial ecosystem model estimates

Yaling Liu[1], Qianlai Zhuang[1,2], Diego Miralles[3,4], Zhihua Pan[5], David Kicklighter[6], Qing Zhu[7], Yujie He[1], Jiquan Chen[8], Nadja Tchebakova[9], Andrey Sirin[10], Dev Niyogi[1,2], and Jerry Melillo[6]

[1]Department of Earth, Atmospheric, and Planetary Sciences, Purdue University, West Lafayette, Indiana, USA, [2]Department of Agronomy, Purdue University, West Lafayette, Indiana, USA, [3]Department of Earth Sciences, VU University Amsterdam, Amsterdam, Netherlands, [4]Laboratory of Hydrology and Water Management, Ghent University, Ghent, Belgium, [5]College of Resources and Environmental Sciences, China Agricultural University, Beijing, China, [6]Ecosystems Center, Marine Biological Laboratory, Woods Hole, Massachusetts, USA, [7]Climate Sciences Department, Earth Sciences Division, Lawrence Berkeley National Laboratory, Berkeley, California, USA, [8]CGCEO/Geography, Michigan State University, East Lansing, Michigan, USA, [9]V N Sukachev Institute of Forest, Siberian Branch, Russian Academy of Sciences, Krasnoyarsk, Russia, [10]Laboratory of Peatland Forestry and Amelioration, Institute of Forest Science, Russian Academy of Sciences, Uspenskoye, Russia

Abstract The ecosystems in Northern Eurasia (NE) play an important role in the global water cycle and the climate system. While evapotranspiration (ET) is a critical variable to understand this role, ET over this region remains largely unstudied. Using an improved version of the Terrestrial Ecosystem Model with five widely used forcing data sets, we examine the impact that uncertainties in climate forcing data have on the magnitude, variability, and dominant climatic drivers of ET for the period 1979–2008. Estimates of regional average ET vary in the range of 241.4–335.7 mm yr^{-1} depending on the choice of forcing data. This range corresponds to as much as 32% of the mean ET. Meanwhile, the spatial patterns of long-term average ET across NE are generally consistent for all forcing data sets. Our ET estimates in NE are largely affected by uncertainties in precipitation (*P*), air temperature (*T*), incoming shortwave radiation (*R*), and vapor pressure deficit (VPD). During the growing season, the correlations between ET and each forcing variable indicate that *T* is the dominant factor in the north and *P* in the south. Unsurprisingly, the uncertainties in climate forcing data propagate as well to estimates of the volume of water available for runoff (here defined as P-ET). While the Climate Research Unit data set is overall the best choice of forcing data in NE according to our assessment, the quality of these forcing data sets remains a major challenge to accurately quantify the regional water balance in NE.

1. Introduction

Evapotranspiration (ET) is an essential physical process that governs the energy, water, and carbon cycling between land and atmosphere [*Dolman and De Jeu*, 2010; *Wang and Dickinson*, 2012]. Direct measurements of ET only exist at local scales, making the accurate large-scale modeling of this flux a necessary task to improve management of water resources and reduce uncertainties in our predictions of the hydrosphere's response to climate change. However, ET modeling is cumbersome due to the large number of biogeophysical (e.g., soil moisture, plant physiology, and soil properties) and meteorological (e.g., radiation, temperature, humidity, and wind speed) factors affecting this natural process [*Monteith*, 1965; *Niyogi et al.*, 2009; *Dolman and De Jeu*, 2010]. Nevertheless, recent years have seen the development of process-based numerical models that represent the key physical and biogeochemical interactions driving ET, including: hydrological models [e.g., *Vörösmarty et al.*, 1998], dynamic vegetation models [e.g., *Sitch et al.*, 2003], land surface models [e.g., *Liang et al.*, 1994; *Niu et al.*, 2011], or simple algorithms designed to run with satellite Earth observations as input [*Mueller et al.*, 2013; *McCabe et al.*, 2013]. These numerical models enable the estimation of ET at regional or global scales, at various spatial and temporal resolutions, and with different degrees of accuracy.

The accuracy in ET estimates from numerical models depends on (a) the accuracy in the climate data used to force the models, (b) the realism of the model representations of the physical and biogeochemical processes that occur in nature, and (c) the spatiotemporal scale and resolution of the ET estimates. Previous studies have investigated these sources of uncertainty. For example, *Douville* [1998] examined the sensitivity of ET to

the changes in land surface parameters, precipitation forcing, and runoff representation. While *Douville* [1998] used a single land surface model, *Oki et al.* [2006] uncovered large discrepancies in the ET estimates from a range of models. Likewise, *Rawlins et al.* [2006] investigated the effects of different forcings and methods for the estimation of ET in the Western Arctic. More recently, both *Livneh and Lettenmaier* [2012] and *Ferguson et al.* [2010] reported how a lack of water availability constraints on remote sensing ET estimates might lead to overestimations of the flux. Along with many others, these studies highlighted the requirement of both high-quality forcing data and sound model representation for the accurate estimation of ET. Nonetheless, the sensitivity of *ET* estimates to forcing uncertainties is expected to change from region to region, and a detailed study of the impact of these forcing uncertainties on ET estimates over Northern Eurasia (NE) is still missing.

NE is a critical region for Earth's climate due to its vast area, its high sensitivity to global warming [*Serreze et al.*, 2000; *Intergovernmental Panel on Climate Change*, 2007], and its significant feedbacks on the global climate system [*Adam and Lettenmaier*, 2008; *Groisman et al.*, 2010]. NE accounts for 19% of the Earth's land surface and contains about 70% of the Earth's boreal forests and more than two thirds of the Earth's permafrost [*Northern Eurasia Earth Science Partnership Initiative* (*NEESPI*), 2004]. The hydrological cycle in NE plays an important role in the global climate system. For example, recent increases in the total terrestrial freshwater flux from NE into the Arctic Ocean have been suggested as the cause for the weakening of the Atlantic thermohaline circulation [*Rahmstorf and Ganopolski*, 1999] and the slowdown of the transport of CO_2 to the deep ocean [*Arctic Climate Impact Assessment*, 2005]. Despite the critical importance of NE for the Earth's climate system, the large-scale hydrological patterns of the region remain largely unstudied, especially from the perspective of the interactions between ET and climate.

Here we use an improved version of a process-based biogeochemical model, the Terrestrial Ecosystems Model (TEM 5.0) [*Zhuang et al.*, 2010; *Liu et al.*, 2013, 2014], to estimate ET based on a range of current climate data sets as forcing. This study aims to investigate the plausible ET dynamics in NE during 1979–2008, the range of variability in ET estimates that responds to uncertainties in forcing data, and the regional changes in the sensitivity of ET to different climatic drivers. The overarching goal is to shed light on the appropriateness of currently existing climate forcing data for quantifying the terrestrial water cycle in NE.

2. Methods

2.1. Approach

We use the improved version of TEM by *Liu et al.* [2014] that explicitly considers ET from different land covers: uplands, wetlands, water bodies, and land covered by snow. The ET from uplands and wetlands includes transpiration, evaporation from wet canopies, and evaporation from moist and wet soils. The ET from uplands is constrained by soil water availability, whereas wetlands are considered to have unlimited water available for evaporation. The algorithms for each ET component are based on the Penman-Monteith equation, except for the case of snow sublimation. ET for each land cover type is calculated separately; grid cell aggregates used in this study are based on the average of ET from all land covers weighted by their fractional coverage at each pixel. The fractional coverage of uplands, wetlands, and water bodies are assumed to remain unchanged within each grid cell and add up to one, whereas the fractional snow cover varies monthly. The model solves the surface energy budget to derive surface net radiation; thus, it requires input of incoming shortwave radiation (R), albedo, net emissivity between the atmosphere and the ground, and air temperature (T) [*Mu et al.*, 2011; *Liu et al.*, 2013].

The model was calibrated using measurements from 13 eddy covariance (EC) sites in NE. The calibrated parameters include specific leaf area, mean potential stomatal conductance per unit leaf area (C_L), leaf-scale boundary layer conductance (gl_bl), and coefficients for calculating net emissivity between the atmosphere and ground (a_e and b_e) [*Mu et al.*, 2011; *Liu et al.*, 2014]. This model has also been evaluated using a variety of satellite-based ET products and river discharge measurements from the six largest watersheds in NE. As a result of these evaluations, we have gained confidence in the ability of the model to estimate the spatial and temporal variability in ET over our study region. The ET algorithms, model parameterizations, and validation activities are described in further detail in *Liu et al.* [2014].

The choice of TEM for our study over other existing models is justified for two reasons. First, most ET estimation schemes [*Mengelkamp et al.*, 2006; *Mueller et al.*, 2013] do not explicitly consider some of the

detailed ET processes incorporated in the current version of TEM (e.g., snow sublimation and wetlands), which seem crucial to increase the realism of ET estimates at high latitudes [*Liu et al.*, 2014]. Second, site level comparisons against EC data indicate that the ET derived from the latest TEM version (hereafter called TEM ET) driven by measured meteorological data at the EC sites shows a good performance over NE as opposed to other widely used ET products [see *Liu et al.*, 2014].

Here TEM is run for 1979–2008 using a set of five different climate forcing data sets as indicated in section 2.2, with a spatial resolution of 0.5° latitude × 0.5° longitude. Regional annual estimates from two global satellite-based ET products—the mean of the LandFlux-EVAL merged data sets by *Mueller et al.* [2013], hereafter referred to as EVAL and GLEAM (Global Land surface Evaporation: the Amsterdam Methodology) [*Miralles et al.*, 2011a, 2011b] are used for comparison. Because the primary objective of this study is to examine forcing-induced ET estimation uncertainty using a single model—rather than to investigate disparities among different models—only TEM is involved in the simulations with five different forcing data sets. Additionally, runoff measurements for the six largest watersheds in NE from *Peterson et al.* [2002] and the Global Runoff Data Center (GRDC) are used to evaluate the forcing-induced uncertainties in estimates of P-ET (i.e., a proxy for the volume of water available for runoff; see, e.g., *Miralles et al.* [2011b]. Finally, to identify the dominant drivers of ET in NE, correlations between ET estimates and each forcing variable are calculated, general linear regression models are applied to examine the effects of different forcing data sets and climatic variables on *ET*, and results are contrasted through an analysis based on Budyko curves [*Budyko*, 1974].

2.2. Data

Forcing data of monthly air temperature (*T*), precipitation (*P*), incoming shortwave radiation (*R*) (or alternatively cloudiness, *C*), vapor pressure (*e*), and wind speed (*u*) are needed to drive TEM, along with other ancillary inputs including atmospheric CO_2 concentrations, soil texture, albedo, elevation, and land cover. Climatic inputs vary over time and space, whereas soil texture, elevation, and land cover data vary only spatially and are assumed to be static throughout the 1979–2008 period.

Five widely used climate data sets are used to force TEM and estimate ET for NE: (1) the Climate Research Unit (CRU) TS3.1 (with the *P* data set being the corrected version v3.10.01) from the University of East Anglia [*Harris et al.*, 2013], (2) the European Centre for Medium-Range Weather Forecasts (ECMWF) ERA-Interim Reanalysis [*Dee et al.*, 2011], (3) the National Aeronautics and Space Administration Modern Era Retrospective-Analysis for Research and Applications (MERRA) [*Rienecker et al.*, 2011], (4) the National Centers for Environmental Prediction/National Center for Atmospheric Research (NCEP/NCAR) reanalysis [*Kistler et al.*, 2001], and (5) the Global Meteorological Forcing Data set for land surface modeling from Princeton University (PU) [*Sheffield et al.*, 2006].

Input climate data include monthly average *T, P, R* (or *C*), *V*, and *u*. In the case of the CRU TS3.1 data set, only a monthly climatology is available for *u* (mean of all the same months of the year for 1961–1990, *New et al.* [1999]), and *R* is estimated based on latitude, date, and CRU *C* following *Pan et al.* [1996]. All forcing climate data are resampled at 0.5° spatial resolution by using inverse distance weighted interpolation [*Shepard*, 1968]. We use the soil texture (i.e., sand, silt, and clay percentage) from the Food and Agriculture Organization/Civil Service Reform Committee digitization of the *FAO-UNESCO* [1971] soil map [*Zobler*, 1986]. The distribution of plant functional types (PFTs) is derived from the International Geosphere-Biosphere Program Data and Information System (DIS) DISCover Database [*Belward et al.*, 1999; *Loveland et al.*, 2000] and translated to the TEM vegetation classification scheme [*Melillo et al.*, 1993, see Figure 1]. The distributions of wetlands and water bodies are extracted from the Global Lakes and Wetlands Database (GLWD-3) [*Lehner and Döll*, 2004] and are also translated to the TEM vegetation classification scheme [*Melillo et al.*, 1993]. The fractional coverages of wetlands and water bodies within each 0.5° × 0.5° grid cell are derived based on their distribution in GLWD-3, and the remaining fraction is attributed to uplands covered by various PFTs (i.e., the fraction coverages of uplands, wetlands, and water bodies add up to one, Figure 1). We use the same ancillary data including elevation, albedo, snow cover, and atmospheric CO_2 concentrations, as in *Liu et al.* [2014].

2.3. Study Region

The study domain (Northern Eurasia, NE) includes the former Soviet Union, Northern China, Mongolia, Fennoscandia, and Eastern Europe (Figure 1) [*NEESPI*, 2004]. Low winter temperature over most of the continent and aridity in its southern part are the two main climatic features [*Shahgedanova*, 2002]. There is a
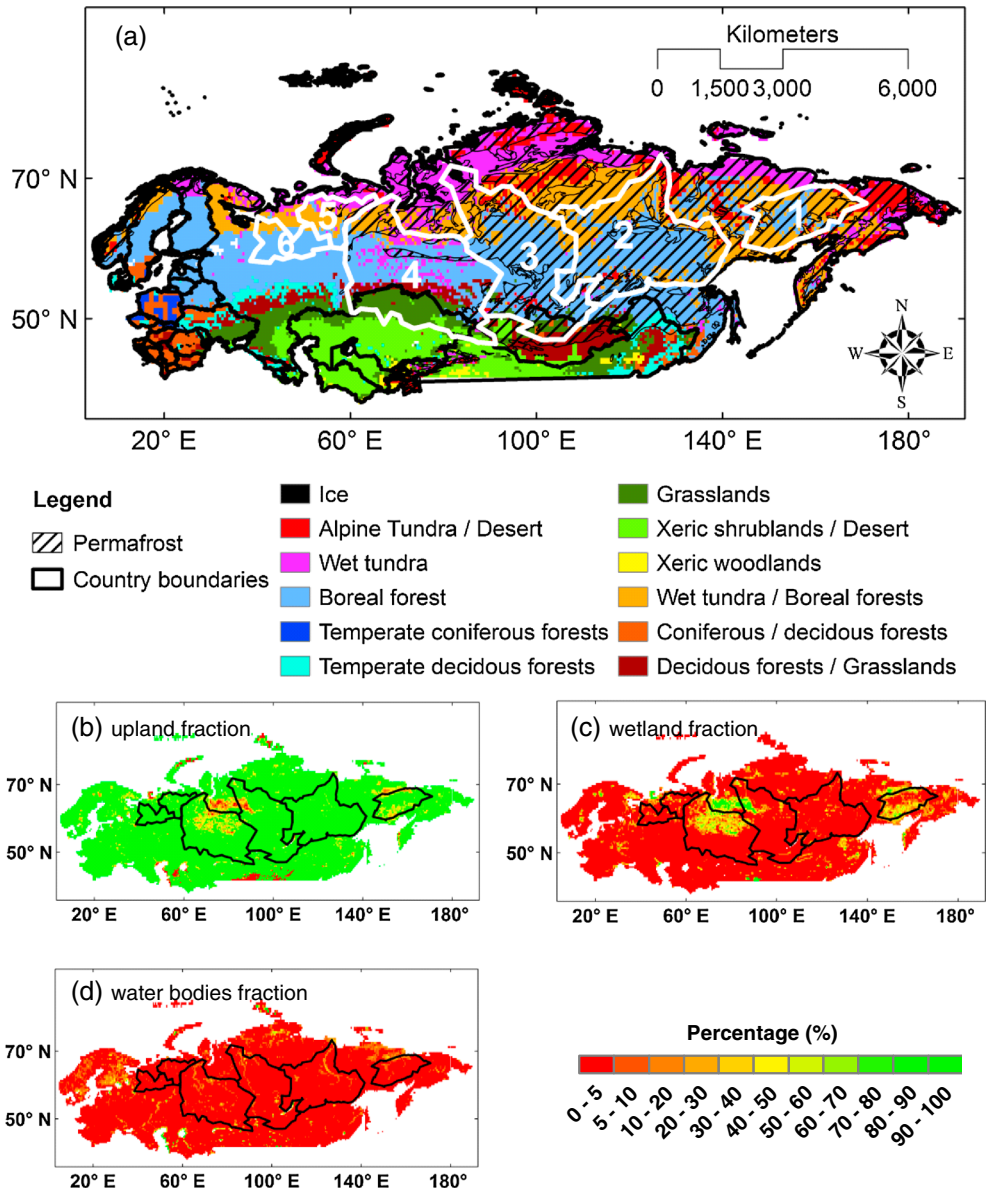
Figure 1. Distribution of plant functional types (PFT) in (a) the NE domain, and fractional coverage of (b) upland ecosystems, (c) wetlands, and (d) water bodies. The boundaries of six major river watersheds in the NE domain are delineated (1, 2, 3, 4, 5, and 6 stand for Kolyma, Lena, Yenisei, Ob, Pechora, and Northern Dvina watersheds, respectively). Permafrost extension is marked by the hatched lines.

decreasing temperature gradient from the west to the east, especially during winter, reflecting an increased climate continentality (e.g., mean January temperatures vary from −1°C along the western border of the former Soviet Union to −50°C in eastern Siberia). Annual precipitation is variable and heterogeneously distributed; mean volumes for the entire NE domain show an interannual range of 300–800 mm yr^{-1}, with as little as 30 mm yr^{-1} during some years in parts of central Asia and more than 2500 mm yr^{-1} in western Transcaucasia [*Shahgedanova*, 2002]. Around 44% of the land area is covered by permafrost, covering most of Siberia (see Figure 1a) [*Brown et al.*, 1998]. The region contains six major river watersheds: Kolyma, Lena, Yenisei, Ob, Pechora, and Northern Dvina (Figure 1). While the tundra covers the northernmost lands of the domain up to the Arctic shore, boreal forests are situated between 45 and 70°N [*Larsen*, 1980], and steppes occur to the south of the boreal forest (see again Figure 1). In our analyses, we consider the southern extent of the boreal forest as the boundary between the north and the south domains.

Table 1. Observed Data at Meteorological Stations and EC Sites Used to Assess the Forcing Data Sets[a]

Spatial domain	Data Sets	Time Span	Temporal Resolution	Number of Stations	Data Source
Europe	T	1979–2008	Daily	1637	ECA&D
Europe	P	1979–2008	Daily	2718	ECA&D
Europe	RH	1979–2008	Daily	192	ECA&D
Europe	C	1979–2008	Daily	500	ECA&D
Europe	u	1979–2008	Daily	92	ECA&D
China	P, T, RH, u	1981–2008	Monthly	175	CMA
NE (EC sites)	P, T, e, R	2000–2008	Half hour	12	http://www.asianflux.com, http://gaia.agraria.unitus.it/

[a]Time series data at different temporal resolutions are resampled to a monthly resolution. T = Air temperature, P = Precipitation, e = Vapor pressure, R = Incoming solar radiation, C = Cloudiness, u = Wind speed, RH = Relative humidity.

3. Results

3.1. Temporal and Spatial Uncertainties in Forcing Data

Grid cell data from the five forcing data sets are evaluated against the observed meteorological data from the European Climate Assessment & Dataset (ECA&D), the National Meteorological Information Center of China Meteorological Administration (CMA), and eddy covariance (EC) towers within the NE domain (Table 1). The temporal variability of the climate forcing variables differs substantially among the data sets (Figure 2). Overall, ERA-Interim shows the highest T, VPD, and u; NCEP/NCAR has the highest P and R; and CRU shows the lowest values of P, T, and R. In MERRA, u is systematically lower than all the other data sets. Aside from
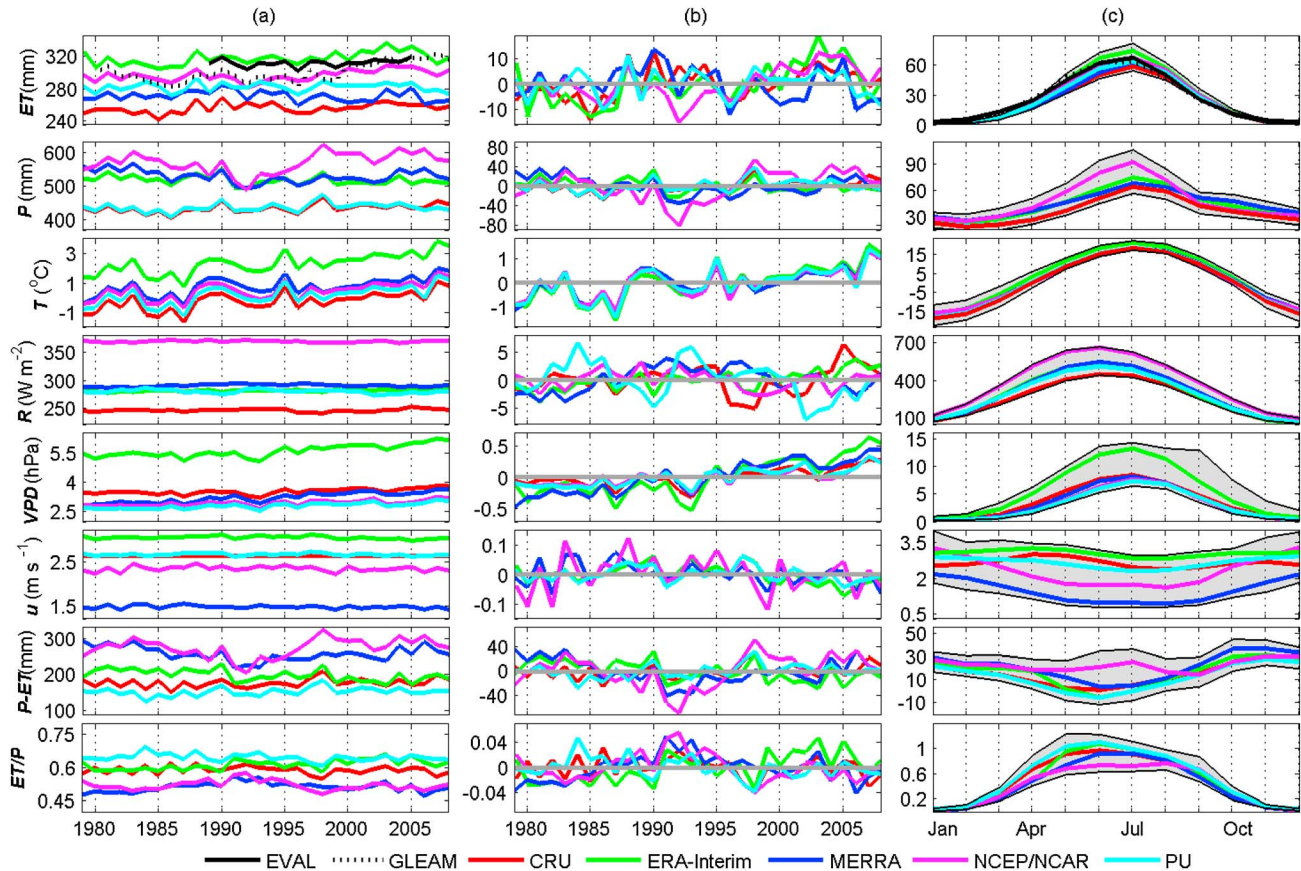

Figure 2. Temporal variability of the regional TEM ET and forcing variables in the NE. (a) Interannual variability, (b) annual anomaly, and (c) climatological seasonal cycle (calculated by averaging all the same months of the year for 1979–2008). The shaded area represents the spread of the monthly values (the difference between the largest and lowest values for each month over 1979–2008).
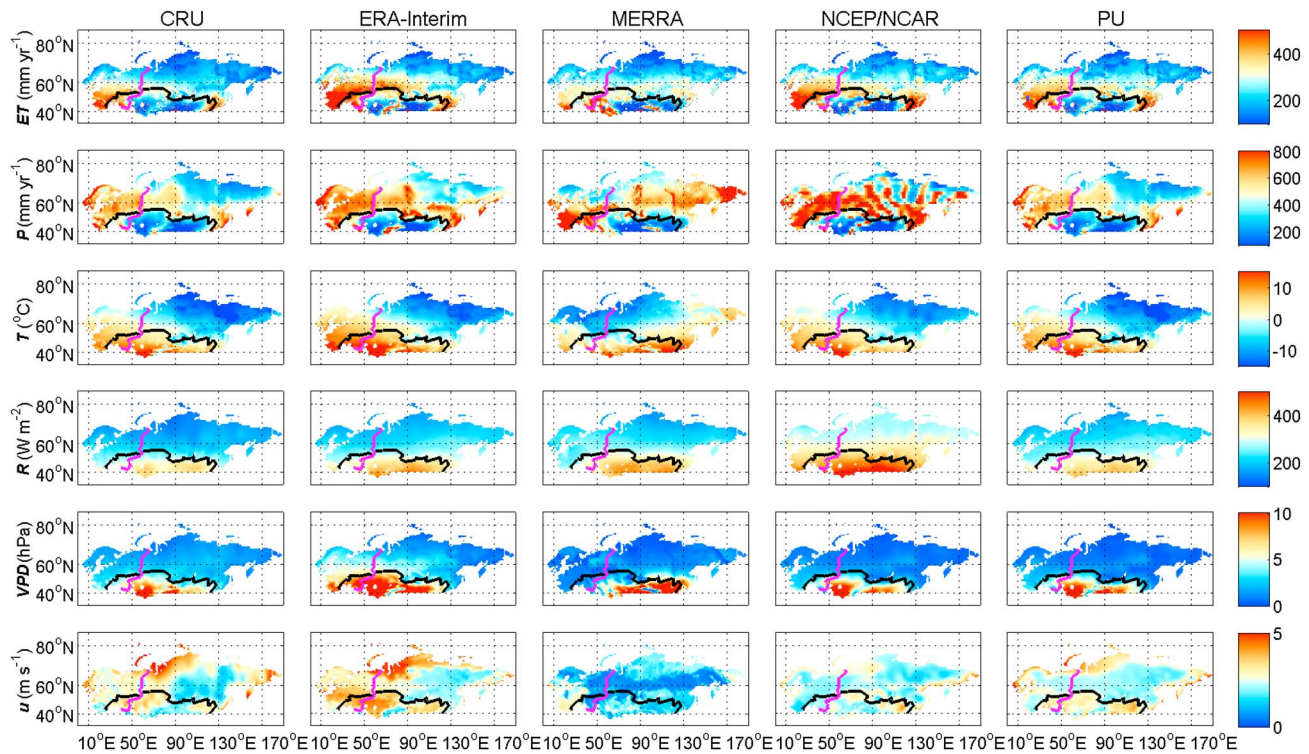
Figure 3. Spatial variability of the TEM ET and forcing variables in the NE; here average annual values during 1979–2008 are presented. The black line on the map represents the boundary between the north and south (south extent of the boreal forest), and the pink line is the boundary between Asia NE and Europe NE.

systematic errors, the temporal dynamics of T, VPD, and u are remarkably similar for all five forcing data sets. In contrast, P and R show larger differences, with correlation coefficients (r) between different data sets ranging from 0.25 to 0.90 for P, and even lower (−0.11–0.45) for R (see also Figure 2b). In terms of long-term (1979–2008) average spatial variability over the study region, the different forcing data sets agree better with each other than they do in time. The large differences in the spatial distribution from forcing to forcing only occur for u (Figure 3).

Comparison against in situ measurements reveals an overall better quality of the CRU TS3.1 data set (Table 2), with the best statistical metrics of all five data sets for T, P, and relative humidity (RH) (derived from T and e after *Andrews* [2010]). Conversely, ERA-Interim shows the highest average root-mean-square error (RMSE) for T, NCEP/NCAR for P, and MERRA for RH and u. ERA-Interim shows the lowest average RMSE for u. At the same time, MERRA displays the lowest correlation with measurements for most climate variables (T, P, RH, and u).

It must also be noted that the scale mismatch between the gridded forcing data sets and the in situ measurements may be inherently reflected in the results of this validation. In addition, whether the available

Table 2. Evaluation of the Forcing Data Against Observations at Meteorological Stations and EC Sites[a]

	CRU			ERA-Interim			MERRA			NECP/NCAR			PU		
	RMSE	MPE	r	RMSE	MPE	r	RMSE	MPE	r	RMSE	MPE	r	RMSE	MPE	r
T	1.28	9.2%	0.99	2.2	14.2%	0.98	1.91	22.7%	0.91	1.66	12.9%	0.98	1.31	8.1%	0.98
P	11.9	16.8%	0.84	14.1	22.1%	0.82	14.5	27.8%	0.31	20.2	36.1%	0.66	13.4	18.7%	0.81
RH	8.2	4.5%	0.68	11.5	12.5%	0.79	15.8	17.8%	0.11	10.7	12%	0.55	14.4	12.3%	0.25
u[b]	N/A	N/A	N/A	1.3	37.4%	0.67	1.9	48.3%	0.11	1.6	33.2%	0.35	1.49	34.3	0.51
C[b]	10.5	3.5%	0.63	N/A	N/A	N/A	N/A	N/A	N/A	N/A	N/A	N/A	N/A	N/A	N/A

[a]The values represent the average RMSE, average absolute MPE, and average r across all meteorological stations and EC sites. The RMSE units for T, P, and u are °C, mm mon^{-1}, and m s^{-1}, respectively, while RH and C are expressed in %. T = air temperature, P = precipitation, RH = relative humidity, C = cloudiness, u = wind speed.
[b]Statistics for u are not available for CRU because CRU does not have monthly time series data, and statistics for C are only available for CRU because R is collected instead of C for the other four data sets. Here R is not assessed due to shortage of in situ measurements.

Table 3. Standard Deviation (σ) of Different ET Products and Forcings Over 1979–2008[a]

	$\sigma1$	$\sigma2$	CRU		ERA-Interim		MERRA		NCEP/NCAR		PU	
			$\sigma3$	$\sigma4$	$\sigma3$	$\sigma4$	$\sigma3$	$\sigma4$	$\sigma3$	$\sigma4$	$\sigma3$	$\sigma4$
ET	21.3	134.6	6.1	117.3	8.1	162.0	6.5	118.1	6.6	133.9	5.3	126.3
P	54.1	251.0	12.8	212.0	13.6	220.8	19.1	253.0	29.8	311.5	12.8	212.5
T	0.9	8.1	0.6	8.4	0.7	9.0	0.6	7.2	0.6	7.2	0.6	8.4
R	40.8	81.1	2.5	69.3	1.8	72.1	2.2	75.0	1.6	73.2	3.2	61.3
VPD	1.0	3.3	0.1	2.3	0.3	4.3	0.3	3.3	0.1	2.7	0.1	2.8
u	0.5	0.9	0.0	0.9	0.0	0.9	0.0	0.7	0.1	0.5	0.0	0.7

[a]$\sigma1$: Mean temporal σ of the ensemble of ET products/forcings; $\sigma2$: spatial σ of the ensemble mean of ET products/forcings; $\sigma3$: temporal σ of each particular ET product/forcing; $\sigma4$: spatial σ of each particular *ET* product/forcing. Note that $\sigma2$ and $\sigma4$ are calculated based on the mean ET map over 1979–2008 (i.e. Figure 3). The units for ET, *P, T, R*, VPD, and *u* are mm yr^{-1}, mm yr^{-1}, °C, W m^{-2}, hPa, and m s^{-1}, respectively.

in situ stations are representative for the entire NE region may be put in question; e.g., although the spatial patterns of *P* and *T* differ between MERRA and NCEP/NCAR, their average RMSEs (against in situ) are similar. This arises from the fact that no ground weather stations in Siberia are involved in the assessment of forcing data sets due to the inaccessibility of time series data in that area (Table 1), where the disagreement between the two data sets is the largest (see Figure 3). Despite these scale and representativeness issues, our assessment still offers important overall insights with respect to the accuracy of the forcing data relative to ground observations and also reveals large discrepancies among the different forcing data sets.

For most variables, the standard deviation (σ) of the forcing data ensemble is larger than the σ of each forcing data set (Table 3). This holds for both temporal and spatial σ, suggesting that the uncertainties in the forcings may be higher than the (estimated) dynamic range of these variables. Especially, the mean temporal σ of the forcing ensemble for *R* and *u* is up to 25 and 17 times the σ of the individual *R* and *u* time series, respectively. Also notable is the spatial σ of *P* in NCEP/NCAR, which is much greater than that of the multiforcing ensemble, suggesting an unrealistically high spatial variability of *P* in NCEP/NCAR, consistent with its large RMSE in Table 2.

3.2. Temporal Uncertainties in ET

The temporal variability of the regional average ET (i.e., area-weighted ET across all grid cells in NE) shows that the annual ET varies substantially from forcing to forcing (Figure 2a); the order from higher to lower values is: ET_{ERA}, ET_{NCEP}, ET_{PU}, ET_{MERRA}, ET_{CRU} (subscripts indicate the forcing used in the derivation of the ET via TEM). While the highest (ET_{ERA}) ranges between 303.9 and 335.7 mm yr^{-1}, the lowest (ET_{CRU}) ranges between 241.4 and 268.7 mm yr^{-1}; these differences of about 32% of the mean magnitude of the flux indicate the potential of forcing uncertainties to induce systematic errors in the ET estimates. Moreover, the mean temporal σ of the ET product ensemble over 1979–2008 is about 3 times higher than the temporal σ of any of the constituent ET products (see Table 3), highlighting once more the importance of this forcing-induced uncertainty in comparison to the real magnitude of the signal. Nonetheless, the discrepancy in the ET estimates from each forcing set appears mostly systematic (see Figure 2a), as an agreement in the temporal dynamics of the ET anomalies from each of the forcing sets still exists (see Figure 2b).

Comparisons to the independent GLEAM satellite-based ET product and LandFlux EVAL synthesis product suggest that the uncertainties in the ET_{NCEP} estimates may be lower. GLEAM reports a spatiotemporal average of 299.5 mm yr^{-1} for NE during 1980–2008, while EVAL reports a value of 311.3 mm yr^{-1} during 1989–2005 (Figure 2a). Note that the better match of ET_{NCEP} to these products is not necessarily a measure of accuracy, as these satellite-based ET data sets also show considerable uncertainties in our study region as recently reported by *Liu et al.* [2014].

Seasonal dynamics are generally similar from product to product independently of the forcing (Figure 2c) and compare well to those of EVAL ($r = 0.95$–0.99) and GLEAM ($r = 0.93$–0.98). Nonetheless, differences still exist in the summer, when solar radiation is at its maximum and evaporative stress is frequent (thus, uncertainties in *P* forcing become crucial). Climatic variables also show the largest discrepancies from forcing to forcing data set in the summer, with an average interforcing spread of *P, T, R*, VPD, and *u* of up to 40.2 mm mon^{-1}, 4.5°C, 227.9 W m^{-2}, 7.2 hPa, and 2.3 m s^{-1}, respectively (Figure 2c). These interforcing differences will
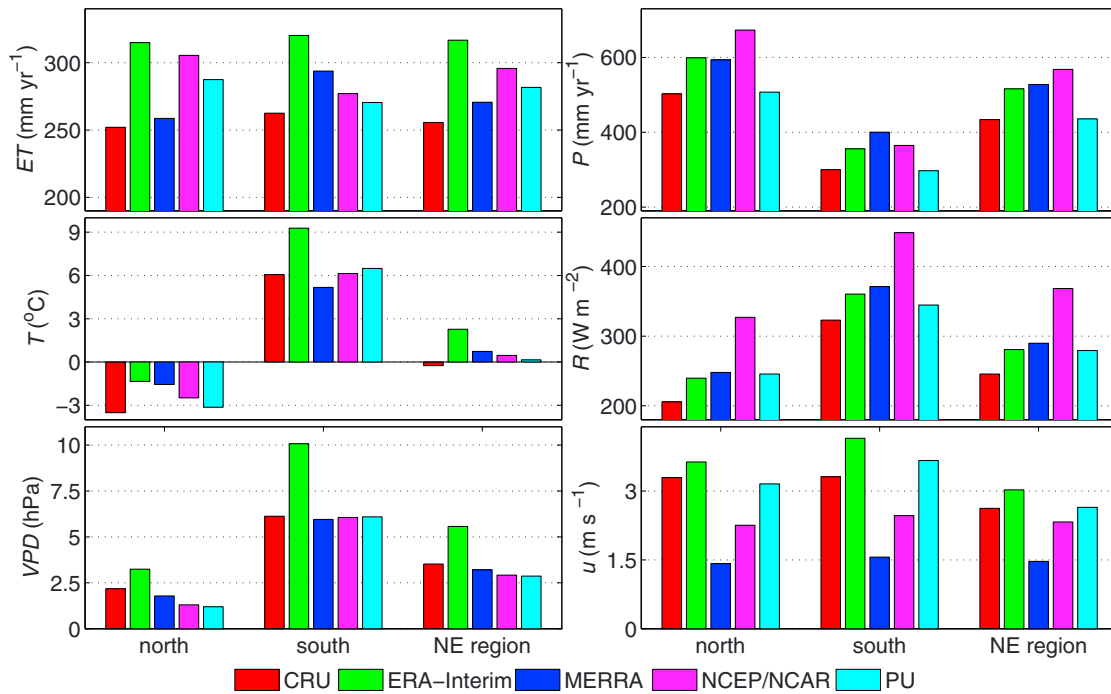
Figure 4. Comparison of the TEM ET and climate forcing across different landscapes in the NE.

inevitably result in large differences in the subsequent ET estimates, as mentioned above. For example, in summertime, ET$_{CRU}$ shows the lowest average values due to the lowest P, T, and R, while ET$_{ERA}$ shows the highest values as a consequence of the high T, P, VPD, and u.

3.3. Spatial Uncertainties in ET

The spatial variability of ET seems more consistent from product to product than the temporal variability, with a common gradient from north to middle latitudes. The highest ET estimates occur in the southwestern temperate forests where energy and water supply are abundant (Figures 1 and 3). The assumption of a static land cover and the observed interforcing agreement in the spatial variability of climatic variables (see Figure 3, section 3.1), likely contribute to the overall consistent spatial variability across the different ET products. Nonetheless, the spatial σ of the ET ensemble is also larger than the spatial σ of each ET product, except for the case of ET$_{ERA}$ (Table 3). The widespread higher and lower values for ET$_{ERA}$ and ET$_{CRU}$, respectively, are likely due to the systematically higher T, VPD, and u in ERA-Interim and systematically lower R and T in the CRU as seen in sections 3.1 and 3.2.

As it can be seen in Figure 4, the differences in mean ET between north and south of NE vary from product to product (see also Table 4). While mean ET is larger in the south than in the north for ET$_{CRU}$, ET$_{ERA}$, and ET$_{MERRA}$, it is the opposite for ET$_{NCEP}$ and ET$_{PU}$. Since land cover and soil properties being used are the same across these products, these spatial discrepancies can be attributed to uncertainties in the forcings. As an example, in MERRA, the atmospheric demand for water in the south is higher (i.e., higher R, T, and u), which results in rates of ET being higher than those in the north.

3.4. Temporal Uncertainties of P-ET

The TEM simulations indicate that the annual mean volumetric soil moisture varied little from year to year in NE, which allows P-ET to be used as a surrogate for the volume of water directed to runoff. For each forcing data set, estimates of P-ET are estimated using the P in the forcing data set minus the ET resulting from running TEM with that forcing data set. Then, the P-ET estimates from the six largest watersheds in the NE (Figure 1) are aggregated to obtain the total runoff for the six watersheds. These aggregated estimates are then compared to river discharge measurements from the GRDC and those by *Peterson et al.* [2002] for the 1979–1999 overlap period. This comparison is done at annual basis to give validity to the underlying

Table 4. Average TEM ET and Climate Forcing Across the North, the South, and NE Region During 1979–2008[a]

	Variable	CRU	ERA-Interim	MERRA	NCEP/NCAR	PU
North	ET	252.1	314.9	258.7	305.4	287.5
	R	205.5	239.7	247.9	327.1	245.6
	P	502.9	599.2	593.6	673.4	507.5
	T	−3.5	−1.4	−1.6	−2.5	−3.1
	VPD	2.2	3.2	1.8	1.3	1.2
	u	3.3	3.6	1.4	2.3	3.2
South	ET	262.5	320.3	293.7	277.1	270.4
	R	322.9	360.3	371.1	448.6	344.6
	P	300.0	355.7	400.3	364.9	297.1
	T	6.1	9.3	5.2	6.1	6.5
	VPD	6.1	10.1	6.0	6.1	6.1
	u	3.3	4.2	1.6	2.5	3.7
NE region	ET	255.6	316.7	270.6	295.8	281.7
	R	245.5	280.8	289.9	368.5	279.4
	P	433.7	516.2	527.8	568.3	435.8
	T	−0.3	2.3	0.7	0.5	0.1
	VPD	3.5	5.6	3.2	2.9	2.9
	u	2.6	3.0	1.5	2.3	2.6

[a]The units of ET, R, P, T, VPD, and u are mm yr^{-1}, W m^{-2}, mm yr^{-1}, °C, hPa, and m s^{-1}, respectively.

assumptions of (a) negligible changes in soil water storage, (b) instantaneous travel time of rainfall to the river outlet, and (c) watertight watersheds.

The average interproduct spread for the P-ET estimates amounts to as much as 2140.1 km^3 yr^{-1}. Likewise, CRU provides the best match of P-ET to the mean in situ river discharge from the GRDC and *Peterson et al.* [2002] (Figure 5). The RMSE and mean percentage error (MPE) for the five P-ET products are: 164.25 km^3 yr^{-1} and −5.43% for CRU; 405.35 km^3 yr^{-1} and 19.77% for ERA-Interim; 492.63 km^3 yr^{-1} and −25.32% for PU; 843.71 km^3 yr^{-1} and 41.62% for MERRA; and 1647.34 km^3 yr^{-1} and 87.88% for NCEP/NCAR. It can be seen that NCEP/NCAR shows a systematic overestimation, in agreement with the positive bias in P illustrated in Figure 2. Meanwhile, different P-ET products present contrasting trends: while (P-ET)$_{NCEP}$ shows an (significant, $p < 0.01$) increasing trend, (P-ET)$_{CRU}$ and (P-ET)$_{PU}$ are untrended, (P-ET)$_{MERRA}$ and (P-ET)$_{ERA}$ present a decreasing trend ($p < 0.01$), contrary to previous findings by *Peterson et al.* [2002]. These results suggest again that the choice of climate forcing is crucial for the adequate modeling of large-scale water resources in the region.

3.5. Dominant Factors in Determining ET

During the growing season (May to September) [see, e.g., *Groisman et al.*, 2003; *Parmentier et al.*, 2011], Pearson's correlation coefficients (r) between each of the five TEM ET products and the corresponding climate
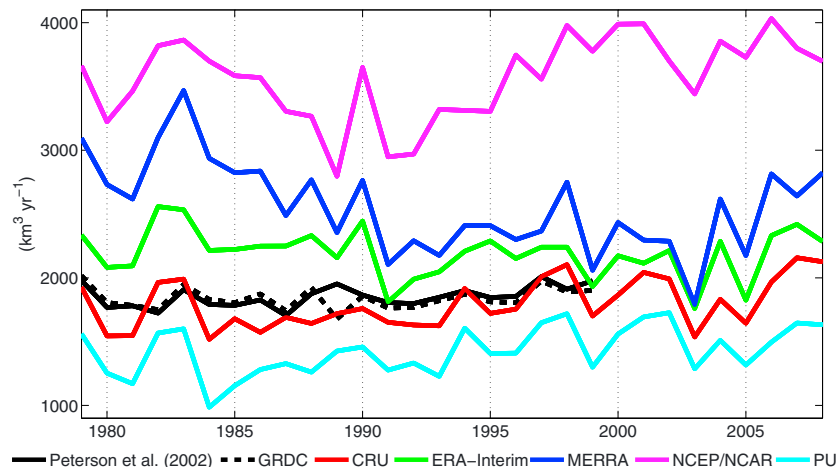

Figure 5. Comparison of TEM *P-ET* estimates driven by the five forcing data sets with the runoff measurements in *Peterson et al.* [2002] and GRDC in the NE region.
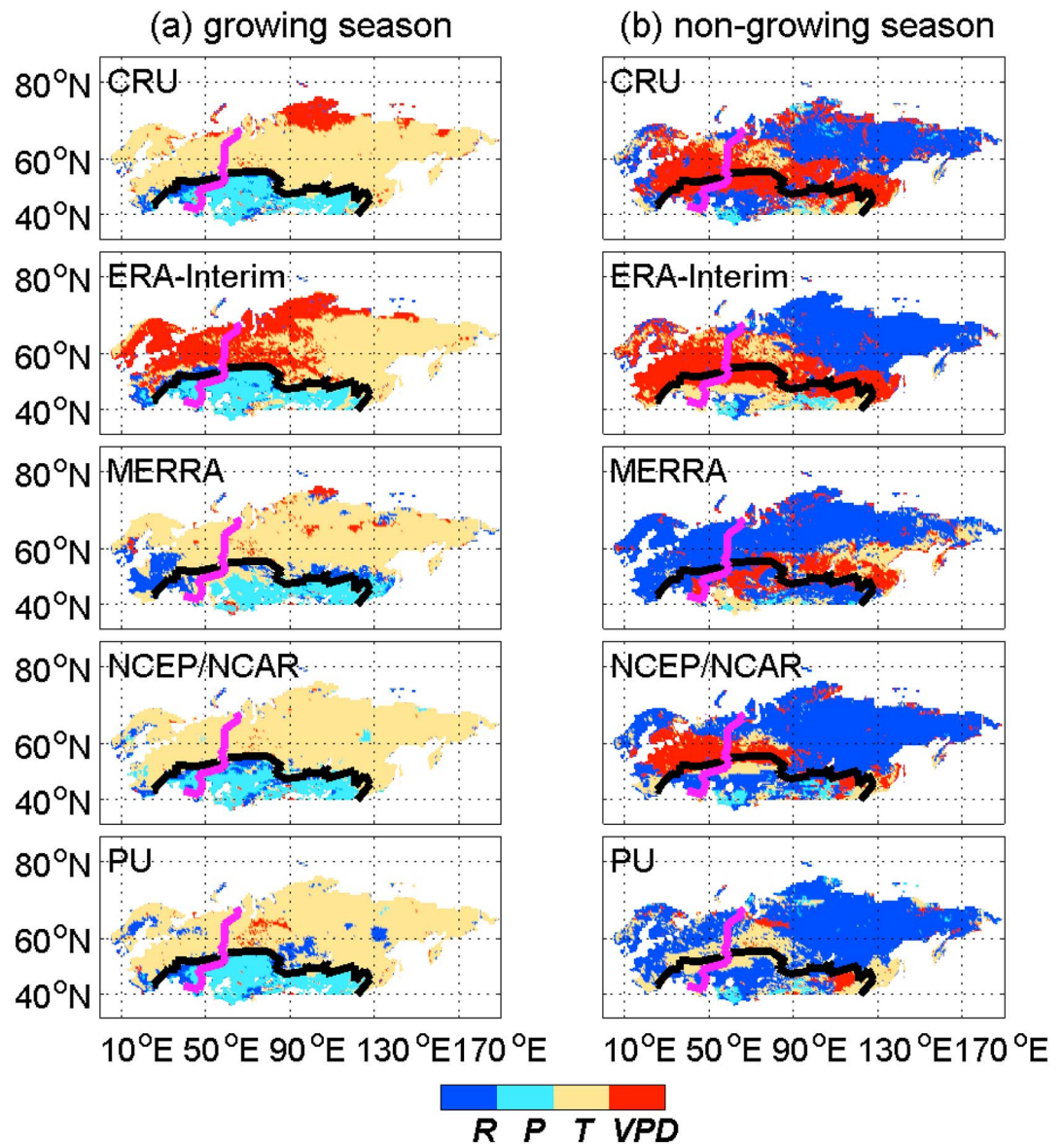
Figure 6. Spatial patterns of climate variables that show the highest Pearson correlation with TEM ET ($p < 0.05$) during (a) the growing season and (b) nongrowing season. Correlations are based on monthly time series for 1979–2008. The black line on the map represents the boundary between the north and south (south extent of the boreal forest), and the pink line is the boundary between Asia NE and Europe NE.

forcing variables unanimously indicate that ET is primarily constrained by T in the north and P in the south (Figure 6a). Nonetheless, T and R are highly correlated in the north ($r = 0.68$–0.91, for the five forcing data sets), indicating that a large fraction of the correlation between ET and T may be explained by the dependency of T (and ET) on R. Out of the growing season, the variability of ET is mainly dominated by R (Figure 6b), partly due to the dependency of snow sublimation on R as represented by the TEM [*Coughlan and Running*, 1997; *Liu et al.*, 2014]. When using the CRU and ERA-Interim forcing, TEM ET is highly correlated to VPD in the southwest during the nongrowing season. Note, however, that the r between VPD and R in this area are also high, indicating the interdependency of these two variables.

Budyko curves [*Budyko*, 1974] derived from the five sets of ET products further confirm the above results (Figure 7). In the south, most grid cells in all five data sets consistently display ratios of potential ET to P (i.e., PET/P) that are greater than 1, suggesting that ET in this region is limited by the supply of water. On the other hand, PET/P is less than 1 in most grid cells of the north, indicating energy limitation. The interproduct
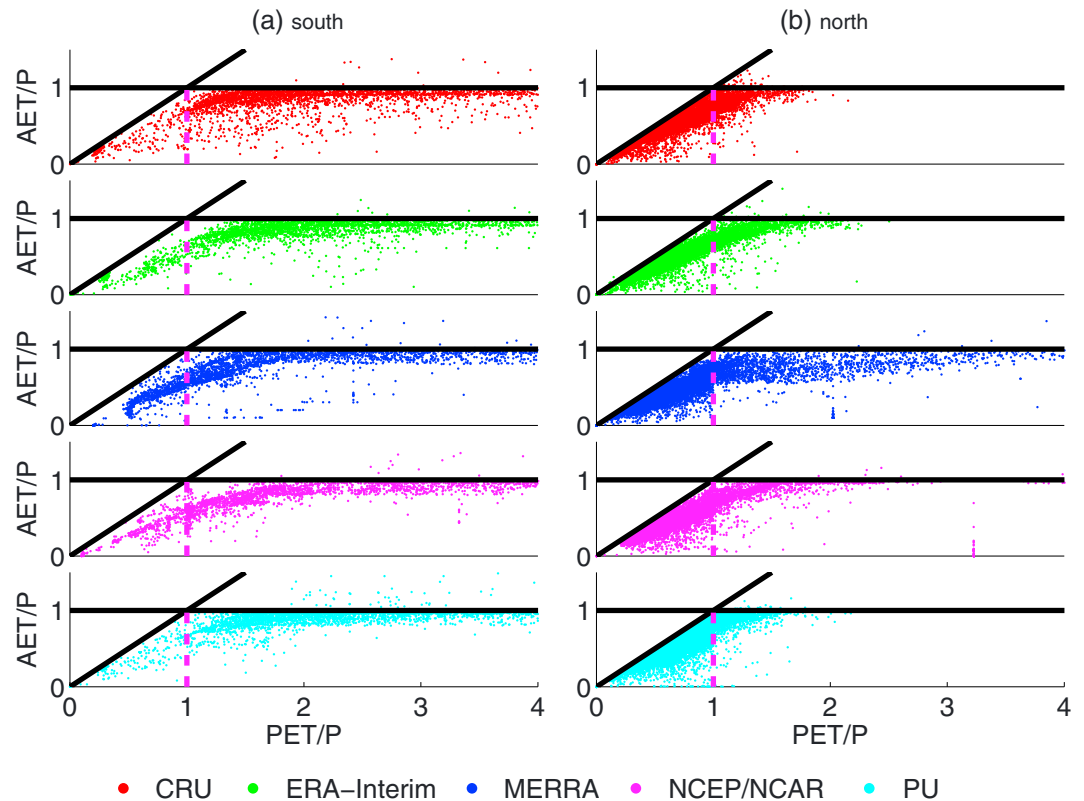
Figure 7. Budyko curves derived using TEM estimates and the five forcing data sets for the (a) south and (b) north. Each point represents a different grid cell. Horizontal axis represents the ratio of potential evapotranspiration to precipitation (PET/P), and the vertical axis stands for the ratio of actual evapotranspiration to precipitation (AET/P).

consistency in the spatial variability of the dominant ET drivers (Figures 6 and 7)—despite the clear differences among the different forcing data sets (see Figures 2, 3, and 4)—indicates the important role played by the static ancillary data sets of soil properties and land use, and especially the ET algorithms and parameterizations, in defining the sensitivity of the model output (ET) to the different forcing variables.

Finally, to further unravel the effects of the different forcing data sets and climatic variables on ET, we apply two general linear regression models (GLMs), one for the north and one for the south. In this analysis, we consider the effects of forcing data sets, climatic variables, and their interactive effects on ET. The ET in each grid cell across NE during 1979–2008 is used as dependent variable, with the ET estimates derived from the five forcings combined into a single GLM. While the five forcing data sets are used as categorical independent variables, each climatic variable (i.e., T, P, R, VPD, and u) from the five data sets is combined and used as continuous independent variable. Results confirm that T is the dominant factor controlling ET in the north (accounting for 69% of model variation, $R^2 = 0.78$) and that the choice of forcing data set has a significant effect on the ET estimates (with 13% of model variation explained by the choice of forcing). For the south, the GLM analysis also supports previous results, with P being the dominant climatic driver of ET. Although the quantitative importance of T in the north and P in the south depends on the data set used as forcing, the choice of forcing data does not lead to qualitative changes in the order of dominant ET drivers.

4. Discussion

Our findings on the controlling factors of ET are generally consistent with previous studies. *Seneviratne et al.* [2010], *Teuling et al.* [2009], and *Miralles et al.* [2011b], all examined the global/continental distribution of water-limited and energy-limited regimes by analyzing correlations of ET against P and R. They based their analysis on simulations from the Global Soil Wetness Project and eddy covariance towers [*Teuling et al.*, 2009], global climate models [*Seneviratne et al.*, 2010], and satellite observations [*Miralles et al.*, 2011b]. They all found a

distinctive boundary in the NE separating an energy-limited regime in the north from a water-limited regime in the south, which is consistent with our findings based on correlations to forcing variables, Budyko curves, and linear regressions. Water limitations in the south indicate the need for accurate precipitation data, thus, suggesting that ET models that are based on energy terms alone [e.g., *Thornthwaite*, 1948; *Turc*, 1961; *Hamon*, 1963] are not appropriate for the estimation of ET in the region. Nevertheless, the control of water availability in the south is mostly restricted to the growing season, in agreement with the results by *Miralles et al.* [2011b].

Uncertainties in model estimates of hydrological fluxes are often considered to be largely induced by uncertainties in forcing data [*Rawlins et al.*, 2006; *Guo et al.*, 2006]. Nonetheless, errors derived from the model assumptions, algorithm simplifications, and parameterizations are also critical [*Oki et al.*, 2006; *Guo and Dirmeyer*, 2006]. For instance, *Slater et al.* [2007] investigated the uncertainties in four major pan-Arctic basins (Lena, Yenisei, MacKenzie, and Ob) using five different land surface models driven by ERA-40 data [*Uppala et al.*, 2005]. Their results showed that the spread of the model ensemble ET estimates represented up to 33% of P and up to 66% of the mean ET. On the other hand, our insights are derived from a single biogeochemical model (i.e., TEM), run by an ensemble of forcings. Therefore, the transfer of our findings to other models might need further examination, as the sensitivity of TEM to the choice of forcing data set may not be the same as for other models.

In addition to the uncertainties in forcing data and the choice of algorithms and parameters, estimates of ET will also be affected by uncertainties rooted in the models' ancillary data. In fact, Figure 2 and 3 suggest an important role of the static ancillary data sets of soil properties and land cover used in TEM, which are common to all simulations: despite the large disagreements among the five sets of TEM ET in their temporal patterns, there is a general consistency in their spatial distribution. While the detailed exploration of the uncertainty in these ancillary data sets, and how this uncertainty propagates to ET estimates, is not the main focus of this study, the relative impacts of land cover and soil type have been tested by means of two-way analysis of variance (ANOVA). The ANOVA has been applied to the north and the south separately and for each of the five sets of TEM ET. In the north, results suggest an important role of land cover (explaining 41%–64% of the variation in ET), while in the south, both PFT and soil type are important (totally explaining 11%–15% of the variation in ET). We note that these results do not imply that the impact of the uncertainties in these ancillary data overshadows the effect of climate forcing uncertainties; future studies should explore the ET variability induced by using an ensemble of ancillary variables in an analogue manner to the analysis of the forcing data impacts presented here.

Apart from the use of a single model and the main focus on forcing data uncertainties, other limitations of this study may include the following: (a) the scarcity of ground weather stations in Siberia that could be used in the assessment of the quality of forcing data sets; (b) simplifications in the estimation of ET by TEM, like the nonconsideration of CO_2 effects on stomatal conductance, or the assumption of potential evaporation over wetlands; (c) the use of a seasonal climatology of wind speed for CRU TS3.1, due to unavailability of monthly time series; (d) the use of coarse spatial resolution forcing data, although most ET processes occur at the smaller scale; and (e) the land cover and land use being assumed to remain unchanged during the study period, despite (e.g.) the increasing frequency of forest fires or the intensification of agriculture in NE in recent decades [*McClelland et al.*, 2004].

In spite of limitations, our study unequivocally highlights important disagreements among broadly used climate forcing data sets and provides evidence of the propagation of these uncertainties to the estimation of hydrological fluxes (in particular ET). Thus, this study underscores the need for high-quality input forcing data to model the large-scale hydrology of NE. From our assessment, the CRU forcing appears to be a better representation of reality than other forcing data sets based on its evaluation against in situ measurements and the fact that it yields the lowest bias in the P-ET estimates when compared to river discharge records. Our results also suggest the need for a thorough validation of the estimates of air temperature from the ERA-Interim reanalysis in NE and the precipitation and radiation data from the NCEP/NCAR reanalysis, due to their apparent deficiencies as manifested in our study.

5. Conclusions

The uncertainties in climate forcing data and how they propagate to ET and P-ET estimates, as well as which are the climatic factors driving ET in Northern Eurasia (NE), have been investigated for the period of 1979–2008 using the TEM biogeochemical model [*Liu et al.*, 2014]. Our main conclusions are as follows:

1. Systematic errors in the range of commonly used forcing data sets can be important, and these errors propagate to the model ET estimates for NE, especially in summertime.
2. The interproduct standard deviation of the ET ensemble (that results from running TEM with the five different forcing data sets) is 3–5 times larger than the standard deviation of any of the constituent products in this ensemble.
3. While uncertainties in the forcing data do not alter substantially the average spatial distribution of the TEM ET estimates across NE (dependent on ancillary data and especially land cover in the north), the regional mean and the temporal variability show a larger dependency on the choice of forcing data set.
4. Forcing uncertainties propagate to the P-ET estimates as shown in an evaluation against in situ measured river discharge from the six largest watersheds in NE, to the point that the sign of the modeled runoff trends depends on the choice of forcing data.
5. The CRU forcing presents an apparent better quality in comparison to in situ meteorological measurements, and it leads to an overall good performance of the model (i.e., agreement of modeled P-ET with observational data).
6. The climatic variables that dominate the temporal variability of ET in NE remain the same among forcing data sets: air temperature in the north (energy limited) and precipitation in the south (water limited) during the growing season; out of the growing season, solar radiation and vapor pressure deficit appear to be more important.

References

Adam, J. C., and D. P. Lettenmaier (2008), Application of new precipitation and reconstructed discharge products to discharge trend attribution in northern Eurasia, *J. Clim.*, *21*(8), 1807–1828.

Andrews, D. G. (2010), *An Introduction to Atmospheric Physics*, Cambridge Univ. Press, New York.

Arctic Climate Impact Assessment (2005), *Arctic Climate Impact Assessment*, 1042 pp., Cambridge Univ. Press, New York.

Belward, A. S., J. E. Estes, and K. D. Kline (1999), The IGBP-DIS global 1-km land-cover data set DISCover: A project overview, *Photogramm. Eng. Remote Sens.*, *65*, 1013–1020.

Brown, J., O. J. Ferrians Jr., J. A. Heginbottom, and E. S. Melnikov (1998), Circum-arctic map of permafrost and ground ice conditions, Digital media, revised 2001, Natl. Snow and Ice Data Cent., Boulder, Colo.

Budyko, M. (1974), *Climate and Life*, Int. Geophys. Ser., Academic Press, New York.

Coughlan, J. C., and S. W. Running (1997), Regional ecosystem simulation: A general model for simulating snow accumulation and melt in mountainous terrain, *Landscape Ecol.*, *12*, 119–136.

Dee, D. P., S. M. Uppala, A. J. Simmons, P. Berrisford, P. Poli, S. Kobayashi, U. Andrae, M. A. Balmaseda, G. Balsamo, and P. Bauer (2011), The ERA-Interim reanalysis: Configuration and performance of the data assimilation system, *Q. J. R. Meteorol. Soc.*, *137*, 553–597.

Dolman, A. J., and R. De Jeu (2010), Evaporation in focus, *Nat. Geosci.*, *3*(5), 296.

Douville, H. (1998), Validation and sensitivity of the global hydrologic budget in stand-alone simulations with the ISBA land-surface scheme, *Clim. Dyn.*, *14*, 151–172.

FAO/UNESCO (1971–1981), *The FAO-Unesco Soil Map of the World*, Legend and 9 volumes, UNESCO, Paris.

Ferguson, C. R., J. Sheffield, E. F. Wood, and H. Gao (2010), Quantifying uncertainty in a remote sensing-based estimate of evapotranspiration over continental USA, *Int. J. Remote Sens.*, *31*, 3821–3865.

Groisman, P. Y., B. Sun, R. S. Vose, J. H. Lawrimore, P. H. Whitfield, E. Førland, I. Hanssen-Bauer, M. C. Serreze, V. N. Razuvaev, and G. V. Alekseev (2003), Contemporary climate changes in high latitudes of the Northern Hemisphere: Daily time resolution, 14th Symp. on Global Change and Climate Variations, CD-ROM 4.8, Am. Meteorol. Soc., Long Beach, Calif.

Groisman, P. Y., G. Gutman, and A. Reissell (2010), Introduction: Climate and land-cover changes in the Arctic, in *Eurasian Arctic Land Cover and Land Use in a Changing Climate*, edited by G. Gutman and A. Reissell, pp. 1–8, Springer.

Guo, Z., and P. A. Dirmeyer (2006), Evaluation of the Second Global Soil Wetness Project soil moisture simulations: 1. Intermodel comparison, *J. Geophys. Res.*, *111*, D22S02, doi:10.1029/2006JD007233.

Guo, Z., P. A. Dirmeyer, Z. Z. Hu, X. Gao, and M. Zhao (2006), Evaluation of the Second Global Soil Wetness Project soil moisture simulations: 2. Sensitivity to external meteorological forcing, *J. Geophys. Res.*, *111*, D22S03, doi:10.1029/2006JD007845.

Hamon, W. R. (1963), Computation of direct runoff amounts from storm rainfall, *Int. Assoc. Sci. Hydrol.*, *63*, 52–62.

Harris, I., P. Jones, T. Osborn, and D. Lister (2013), Updated high-resolution grids of monthly climatic observations—The CRU TS3.10 dataset, *Int. J. Climatol.*, doi:10.1002/joc.3711.

Intergovernmental Panel on Climate Change (2007), *Climate Change (2007), The Physical Science Basis: Contribution of Working Group I to the Fourth Assessment Report of the Intergovernmental Panel on Climate Change*, Cambridge Univ. Press, Cambridge, U. K.

Kistler, R., W. Collins, S. Saha, G. White, J. Woollen, E. Kalnay, M. Chelliah, W. Ebisuzaki, M. Kanamitsu, and V. Kousky (2001), The NCEP-NCAR 50-year reanalysis: Monthly means CD-ROM and documentation, *Bull. Am. Meteorol. Soc.*, *82*, 247–267.

Larsen, J. A. (1980), *The Boreal Ecosystem*, Physiol. Ecol., 500 pp., Academic Press, New York.

Lehner, B., and P. Döll (2004), Development and validation of a global database of lakes, reservoirs and wetlands, *J. Hydrol.*, *296*(1–4), 1–22.

Liang, X., D. P. Lettenmaier, E. F. Wood, and S. J. Burges (1994), A simple hydrologically based model of land surface water and energy fluxes for general circulation models, *J. Geophys. Res.*, *99*, 14,415–14,428, doi:10.1029/94JD00483.

Liu, Y., et al. (2013), Response of evapotranspiration and water availability to changing climate and land cover on the Mongolian Plateau during the 21st century, *Global Planet. Change*, *108*, 85–99.

Liu, Y., et al. (2014), Responses of evapotranspiration and water availability to the changing climate in northern Eurasia, *Clim. Change*, doi:10.1007/s10584-014-1234-9.

Livneh, B., and D. Lettenmaier (2012), Multi-criteria parameter estimation for the unified land model, *Hydrol. Earth Syst. Sci.*, *16*, 3029–3048.

Loveland, T. R., B. C. Reed, J. F. Brown, D. O. Ohlen, Z. Zhu, L. Yang, and J. W. Merchant (2000), Development of a global land cover characteristics database and IGBP DISCover from 1 km AVHRR data, *Int. J. Remote Sens.*, *21*, 1303–1330.

McCabe, M. F., et al. (2013), Global-scale estimation of land surface heat fluxes from space, in *Remote Sensing of Energy Fluxes and Soil Moisture Content*, edited by G. P. Petropoulos, pp. 249–282, CRC Press, New York, doi:10.1201/b15610-13.

McClelland, J. W., R. M. Holmes, B. J. Peterson, and M. Stieglitz (2004), Increasing river discharge in the Eurasian Arctic: Consideration of dams, permafrost thaw, and fires as potential agents of change, *J. Geophys. Res.*, *109*, D18102, doi:10.1029/2004JD004583.

Melillo, J. M., A. D. McGuire, D. Kicklighter, B. Moore, C. J. Vorosmarty, and A. L. Schloss (1993), Global climate change and terrestrial net primary production, *Nature*, *363*(6426), 234–240.

Mengelkamp, H. T., F. Beyrich, G. Heinemann, F. Ament, J. Bange, F. Berger, J. Bösenberg, T. Foken, B. Hennemuth, and C. Heret (2006), Evaporation over a heterogeneous land surface: The EVA-GRIPS project, *Bull. Am. Meteorol. Soc.*, *87*, 775–786.

Miralles, D. G., R. A. M. De Jeu, J. H. Gash, T. R. H. Holmes, and A. J. Dolman (2011a), Magnitude and variability of land evaporation and its components at the global scale, *Hydrol. Earth Syst. Sci.*, *15*(3), 967–981.

Miralles, D. G., R. A. M. De Jeu, J. H. Gash, T. R. H. Holmes, and A. J. Dolman (2011b), Global land-surface evaporation estimated from satellite-based observations, *Hydrol. Earth Syst. Sci.*, *15*(2), 453–469.

Monteith, J. L. (1965), Evaporation and environment, *Symp. Soc. Exp. Biol.*, *19*, 205–224.

Mu, Q., M. Zhao, and S. W. Running (2011), Improvements to a MODIS global terrestrial evapotranspiration algorithm, *Remote Sens. Environ.*, *115*(8), 1781–1800.

Mueller, B., et al. (2013), Benchmark products for land evapotranspiration: LandFlux-EVAL multi-dataset synthesis, *Hydrol. Earth Syst. Sci.*, *17*, 3707–3720.

Northern Eurasia Earth Science Partnership Initiative (2004), The Northern Eurasia Earth Science Partnership Initiative (NEESPI), Executive Overview, Version 2.1.

New, M., M. Hulme, and P. Jones (1999), Representing twentieth-century space-time climate variability. Part I: Development of a 1961–90 mean monthly terrestrial climatology, *J. Clim.*, *12*, 829–856.

Niu, G., et al. (2011), The community Noah land surface model with multi-parameterization options (Noah-MP): 1. Model description and evaluation with local-scale measurements, *J. Geophys. Res.*, *116*, D12109, doi:10.1029/2010JD015139.

Niyogi, D., K. Alapaty, S. Raman, and F. Chen (2009), Development and evaluation of a coupled photosynthesis-based Gas Exchange Evapotranspiration Model (GEM) for mesoscale weather forecasting applications, *J. Appl. Meteorol. Climatol.*, *48*, 349–368.

Oki, T., N. Hanasaki, E. Ikoma, M. Yasukawa, M. Kitsuregawa, and P. A. Dirmeyer (2006), GSWP-2 intercomparison and data distribution center, *GEWEX News*, *16*(3), 11–12.

Pan, Y., A. D. Mcguire, D. W. Kicklighter, and J. M. Melillo (1996), The importance of climate and soils for estimates of net primary production: A sensitivity analysis with the terrestrial ecosystem model, *Global Change Biol.*, *2*(1), 5–23.

Parmentier, F., M. Van Der Molen, J. Van Huissteden, S. Karsanaev, A. Kononov, D. Suzdalov, T. Maximov, and A. Dolman (2011), Longer growing seasons do not increase net carbon uptake in the northeastern Siberian tundra, *J. Geophys. Res.*, *116*, G04013, doi:10.1029/2011JG001653.

Peterson, B. J., R. M. Holmes, J. W. McClelland, C. J. Vorosmarty, R. B. Lammers, A. I. Shiklomanov, I. A. Shiklomanov, and S. Rahmstorf (2002), Increasing river discharge to the Arctic Ocean, *Science*, *298*(5601), 2171–2173.

Rahmstorf, S., and A. Ganopolski (1999), Long-term global warming scenarios computed with an efficient coupled climate model, *Clim. Change*, *43*, 353–367.

Rawlins, M., S. Frolking, R. Lammers, and C. J. Vörösmarty (2006), Effects of uncertainty in climate inputs on simulated evapotranspiration and runoff in the Western Arctic, *Earth Interact.*, *10*, 1–18, doi:10.1175/EI182.1.

Rienecker, M. M., M. J. Suarez, R. Gelaro, R. Todling, J. Bacmeister, E. Liu, M. G. Bosilovich, S. D. Schubert, L. Takacs, and G.-K. Kim (2011), MERRA: NASA's modern-era retrospective analysis for research and applications, *J. Clim.*, *24*, 3624–3648.

Seneviratne, S., T. Corti, E. L. Davin, M. Hirschi, E. B. Jaeger, I. Lehner, B. Orlowsky, and A. J. Teuling (2010), Investigating soil moisture-climate interactions in a changing climate: A review, *Earth Sci. Rev.*, *99*, 125–161, doi:10.1016/j.earscirev.2010.02.004.

Serreze, M. C., J. E. Walsh, F. S. Chapin III, T. Osterkamp, M. Dyurgerov, V. Romanovsky, W. C. Oechel, J. Morison, T. Zhang, and R. G. Barry (2000), Observational evidence of recent change in the northern high-latitude environment, *Clim. Change*, *46*, 159–207.

Shahgedanova, M. (Ed.) (2002), *The Physical Geography of Northern Eurasia*, vol. 3, Oxford Univ. Press, Oxford.

Sheffield, J., G. Goteti, and E. F. Wood (2006), Development of a 50-year high-resolution global dataset of meteorological forcings for land surface modeling, *J. Clim.*, *19*, 3088–3111.

Shepard, D. A. (1968), Two-dimensional interpolation function for irregularly-spaced data, in *Proceedings of the 1968 23rd ACM National Conference*, pp. 517–524, ACM, Princeton, N. J.

Sitch, S., et al. (2003), Evaluation of ecosystem dynamics, plant geography, and terrestrial carbon cycling in the LPJ dynamic global vegetation model, *Global Change Biol.*, *9*, 161–185, doi:10.1046/j.1365-2486.2003.00569.x.

Slater, A. G., T. J. Bohn, J. L. McCreight, M. C. Serreze, and D. P. Lettenmaier (2007), A multimodel simulations of pan-Arctic hydrology, *J. Geophys. Res.*, *112*, G04S45, doi:10.1029/2006JG000303.

Teuling, A. J., et al. (2009), A regional perspective on trends in continental evaporation, *Geophys. Res. Lett.*, *36*, L02404, doi:10.1029/2008GL036584.

Thornthwaite, C. W. (1948), An approach toward a rational classification of climate, *Geogr. Rev.*, *38*, 55–94.

Turc, L. (1961), Evaluation des besoins en eau d'irrigation, évapotranspiration potentielle, *Ann. Agron.*, *12*, 13–49.

Uppala, S. M., et al. (2005), The ERA-40 re-analysis, *Q. J. R. Meteorol. Soc.*, *131*, 2961–3012.

Vörösmarty, C. J., C. A. Federer, and A. L. Schloss (1998), Potential evaporation functions compared on U.S. watersheds: Possible implications for global-scale water balance and terrestrial ecosystem modeling, *J. Hydrol.*, *207*(3–4), 147–169.

Wang, K., and R. E. Dickinson (2012), A review of global terrestrial evapotranspiration: Observation, modeling, climatology, and climatic variability, *Rev. Geophys.*, *50*, RG2005, doi:10.1029/2011RG000373.

Zhuang, Q., J. He, Y. Lu, L. Ji, J. Xiao, and T. Luo (2010), Carbon dynamics of terrestrial ecosystems on the Tibetan Plateau during the 20th century: An analysis with a process-based biogeochemical model, *Global Ecol. Biogeogr.*, *19*(5), 649–662.

Zobler, L. (1986), *A World Soil File for Global Climate Modeling*, NASA Tech. Memo., vol. 87802, NASA, New York.